Spin torque and charge resistance of ferromagnetic semiconductor 2π and π domain walls

E. A. Golovatski and M. E. Flatté

Optical Science and Technology Center and Department of Physics and Astronomy, University of Iowa, Iowa City, Iowa 52242, USA

(Received 22 April 2010; revised manuscript received 21 August 2011; published 23 September 2011)

Charge resistance and spin torque are generated by coherent carrier transport through ferromagnetic 2π domain walls, and follow qualitatively different trends than for π domain walls. The charge resistance of 2π domain walls reaches a maximum at an intermediate wall thickness, unlike π domain walls, whose resistance decreases monotonically with wall thickness. The peak amplitude of the spin torque and the optimal thickness of the domain wall to maximize torque for a 2π wall are more than twice as large as found for a π domain wall in the same material, producing a larger domain wall velocity for the 2π wall and suggesting such walls may be preferable for magnetoelectronic devices incorporating domain wall motion.

DOI: 10.1103/PhysRevB.84.115210 PACS number(s): 72.25.−b, 75.47.−m, 75.50.Pp, 85.75.−d

I. INTRODUCTION

Spin torque generated by spin transport through inhomogeneous magnetic systems, a direct manifestation of the conservation of the angular momentum associated with spin, underlies both unresolved fundamental questions and potential applications, including fast, localized electrical switching of magnetic moments or domains,[1–5] depinning and transport of domain walls,[6–12] electrical driving of ferromagnetic resonance,[13–16] and controlled generation of coherent magnons.[12,17] Structures showing spin torque are commonly domain walls between two regions whose magnetization orientation differs by an angle θ, called θ domain walls. Although spin torque on a π wall has garnered much experimental and theoretical attention,[6,7,18–27] little has been done to explore spin torque in 2π walls, which are known to be stable in many metallic systems,[28] and have been seen experimentally.[29] The difference between 2π wall behavior and π wall behavior might be most marked when ballistic transport across the domain wall is possible, such as for magnetic semiconductor domain walls (whose π walls are predicted to have highly nonlinear dependencies of spin current and charge current on voltage[30,31]). Understanding 2π domain walls may also lead to novel spin torque devices, such have been predicted for π walls.[9,32,33]

Here we calculate the charge and spin transport and torque for π and 2π domain walls in a simplified model of a magnetic semiconductor, whose electronic structure is described with a Stoner model and whose domain walls are spin spirals, either with a uniform spiral angle (abrupt domain wall) or a smoothly varying spiral angle (smooth domain wall). For coherent transport through a uniform spin spiral, analytic solutions for spin-dependent transmission and reflection coefficients for the different spin channels are possible.[30,34] These same solutions can be applied numerically to a smooth domain wall composed of many piecewise uniform spin spirals. Nonlinear voltage dependence of the spin current and spin torque occurs for both the π and 2π walls, but with very different wall-thickness dependence. The 2π domain wall resistance vanishes in the limit of zero thickness as well as for thick walls (in which the spin adiabatically follows the local magnetization), but peaks for intermediate thicknesses; the π domain wall resistance monotonically decreases with thickness. The spin torque on an abrupt π wall weakly depends on domain wall width, except for very thin walls, whereas for a smooth π wall the torque falls off more quickly with thickness. For both abrupt and smooth 2π walls, however, a large spin torque is generated by spin transport over a range of intermediate wall widths, but very little spin torque is generated for both very thin and very thick walls. Even more surprising, the domain wall velocity can be larger for a 2π wall than a π wall, 3π wall, or 4π wall, suggesting that multiple-rotation (helical) walls may provide the fastest domain wall velocities in a ferromagnetic semiconductor material, depending on the domain wall thickness.

II. ANALYTIC MODEL FOR SPIN TRANSPORT THROUGH A DOMAIN WALL

A. Features of the model

Schematics of the π domain wall and 2π domain wall are shown in Fig. 1. There are two regions of ferromagnetic material, with their magnetizations oriented antiparallel for the π wall case and parallel for the 2π wall case, separated by a domain wall. The domain wall is shown as a Neél wall, which is energetically favorable in thin films,[35] but as spin-orbit interactions are neglected here the same physical behavior will occur for the spin transport and torque for a Bloch wall.

This domain wall model has been significantly simplified in order to obtain analytic results. The key approximations are (1) the magnetic material is assumed to be a parabolic-band Stoner model; the spin splitting between spin-up and spin-down is assumed uniform, (2) spin-orbit effects in the electronic structure are neglected, and (3) the structure is assumed to have two leads with a uniform exchange field, separated by a third region with a piecewise constant variation of the exchange field with position. The exchange field in a domain wall is

$$\mathbf{B} = B_0[\sin\theta(x)\hat{\mathbf{x}} + \cos\theta(x)\hat{\mathbf{z}}]. \quad (1)$$

If θ varies smoothly with x in the form $\theta = \phi x/d$, and $\phi = \pi$ or 2π is the angle through which the magnetization rotates from $x = 0$ to $x = -d$ then the domain wall is essentially one or two turns through a spin spiral. A smoother domain wall can also be described in this form, but with piecewise constant spiral angle, as shown in Fig. 2. The spiral angle is chosen to approximate the analytic form for a domain wall in an isotropic Stoner model, $\theta(x) = \sin^{-1}[\tanh(x/\lambda)]$. We find that

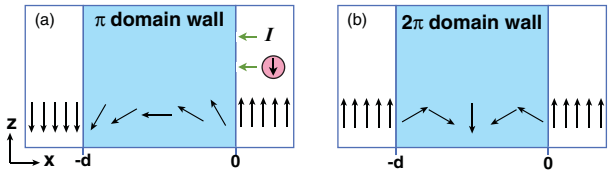

FIG. 1. (Color online) Schematic representation of Néel (a) π and (b) 2π domain walls. Charge transport is assumed to be by holes with spin antiparallel to magnetization.

our results for the smooth wall do not change substantially if the number of piecewise constant regions is doubled compared to that shown in Fig. 2.

The results obtained with these approximations require care when applied to real physical systems. Typical hole-mediated ferromagnetic semiconductors, such as GaMnAs, have nonparabolic and nonspherical bands, nonuniform spin splitting, and substantial spin-orbit interactions. These effects can lead to enhancement of the hole reflectivity and nonadiabatic spin torque for thick π walls, yielding quantitatively different results from those obtained without spin-orbit interaction[21,36–38] in the ballistic limit. Thus differences in the quantitative results for spin-torque for π domain walls calculated using the model here, and those calculated with a GaMnAs electronic structure, suggest that only qualitative trends should be expected, especially for thick walls. There is, however, a clear experimental situation where our first two approximations are quantitatively appropriate—that of a semimagnetic semiconductor with a very large effective g factor, such as ZnMnSe, in the presence of an external magnetic field.[39] The band structure for this system is well described by a uniformly spin-split parabolic band with negligible spin-orbit interaction, and the spatially varying effective exchange field can be induced by the fringe magnetic field from a ferromagnetic domain wall, perhaps deposited as a film on top of the ZnMnSe material.[40]

The abrupt transition from constant to spatially varying exchange field for an abrupt π wall is known to generate a spin torque that is too large and that falls off inversely with the domain wall width, as opposed to the exponential falloff found in a numerical calculation treating a smoothly varying exchange field.[24] We compare the results for the smooth domain wall to those for the abrupt domain wall in Sec. III in order to determine the importance of this effect for 2π walls.

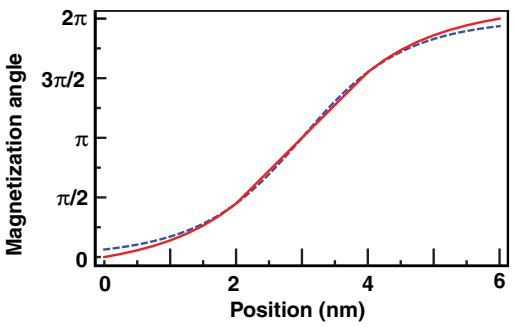

FIG. 2. (Color online) Schematic of a smooth domain wall approximated by 17 piecewise constant spin spirals (solid line). Also shown is the analytic form for a Stoner model, $\theta(x) = \sin^{-1}[\tanh(x/\lambda)]$ (dashed line).

B. Spin-dependent transmission and reflection through the domain wall

We consider spin transport through the domain wall due to holes with spin orientation antiparallel to the material magnetization (as in Fig. 1). These carriers can be reflected or transmitted either with or without flipping their spins. We calculate the reflection and transmission coefficients by solving the Schrödinger equation inside the domain wall[30]:

$$\left[\frac{-\hbar^2}{2m^*}\frac{\partial^2}{\partial x^2} - \frac{\Delta}{2}\begin{pmatrix}\cos\theta(x) & \sin\theta(x)\\ \sin\theta(x) & -\cos\theta(x)\end{pmatrix}\right]\begin{pmatrix}\psi_\uparrow\\ \psi_\downarrow\end{pmatrix} = E\begin{pmatrix}\psi_\uparrow\\ \psi_\downarrow\end{pmatrix}, \tag{2}$$

where Δ is the energy splitting between carriers of opposite spin orientation in the ferromagnetic material. Converting E and Δ into the unitless $\bar{E}$ and $\bar{\Delta}$ by

$$\bar{E} = \frac{2m^*d^2E}{\hbar^2}, \tag{3}$$

$$\bar{\Delta} = \frac{2m^*d^2\Delta}{\hbar^2}, \tag{4}$$

yields

$$\left[-\frac{\partial^2}{\partial x^2} - \frac{\bar{\Delta}}{2d^2}\begin{pmatrix}\cos\theta(x) & \sin\theta(x)\\ \sin\theta(x) & -\cos\theta(x)\end{pmatrix}\right]\begin{pmatrix}\psi_\uparrow\\ \psi_\downarrow\end{pmatrix} = \frac{\bar{E}}{d^2}\begin{pmatrix}\psi_\uparrow\\ \psi_\downarrow\end{pmatrix}. \tag{5}$$

With a position-dependent θ in the Hamiltonian, it is most convenient to transform to a rotating frame.[41] The rotation matrix

$$R = e^{-\frac{i\theta}{2}\sigma_y} = \begin{pmatrix}\cos\frac{\theta(x)}{2} & -\sin\frac{\theta(x)}{2})\\ \sin\frac{\theta(x)}{2} & \cos\frac{\theta(x)}{2}\end{pmatrix}$$

defines $\psi = R\varphi$ and removes the θ dependence from the off-diagonal potential matrix:

$$R^{-1}\begin{pmatrix}\cos\theta(x) & \sin\theta(x)\\ \sin\theta(x) & -\cos\theta(x)\end{pmatrix}R = \sigma_z.$$

The resulting modified Schrödinger equation is

$$\left[-\frac{\partial^2}{\partial x^2} + \frac{i\phi}{d}\sigma_y\frac{\partial}{\partial x} - \frac{\bar{\Delta}}{2d^2}\sigma_z + \frac{\phi^2}{4d^2}\right]\varphi = \frac{\bar{E}}{d^2}\varphi,$$

which has solutions of the form

$$\varphi = e^{ikx}\chi(k), \tag{6}$$

where χ satisfies the equation

$$\left[k^2d^2 - \phi kd\sigma_y + \frac{\phi^2}{4} - \frac{\bar{\Delta}}{2}\sigma_z - \bar{E}\right]\chi = 0, \tag{7}$$

where

$$k_{1,2} = \frac{1}{d}\sqrt{\bar{E} + \frac{\phi^2}{4} \pm \frac{1}{2}\sqrt{\bar{\Delta}^2 + 4\bar{E}\phi^2}} \tag{8}$$

and

$$\chi(k_i) = N_i\begin{pmatrix}-i\phi k_i d\\ \epsilon_i\end{pmatrix}. \tag{9}$$

Here

$$N_i = \frac{1}{\sqrt{{\epsilon_i}^2 + \phi^2{k_i}^2d^2}}, \tag{10}$$

$$\epsilon_i = {k_i}^2 d^2 + \frac{\phi^2}{4} - \frac{\bar{\Delta}}{2} - \bar{E}, \tag{11}$$

and

$$\varphi_{\pm}(k_i) = e^{\pm i k_i x} N_i \begin{pmatrix} \mp i\phi k_i d \\ \epsilon_i \end{pmatrix}. \tag{12}$$

The final expression for φ is

$$\begin{pmatrix} \varphi_1 \\ \varphi_2 \end{pmatrix} = A N_1 e^{i k_1 x} \begin{pmatrix} -i\phi k_1 d \\ \epsilon_1 \end{pmatrix} + B N_1 e^{-i k_1 x} \begin{pmatrix} i\phi k_1 d \\ \epsilon_1 \end{pmatrix} + C N_2 e^{i k_2 x} \begin{pmatrix} -i\phi k_2 d \\ \epsilon_2 \end{pmatrix} + D N_2 e^{-i k_2 x} \begin{pmatrix} i\phi k_2 d \\ \epsilon_2 \end{pmatrix}. \tag{13}$$

The full wave functions inside the domain wall are

$$\psi = R\varphi = \begin{pmatrix} \cos\left(\frac{\phi x}{2d}\right)\varphi_1 - \sin\left(\frac{\phi x}{2d}\right)\varphi_2 \\ \sin\left(\frac{\phi x}{2d}\right)\varphi_1 + \cos\left(\frac{\phi x}{2d}\right)\varphi_2 \end{pmatrix}. \tag{14}$$

The incident and reflected wave functions, expressed in the right hand lead, are

$$\psi_{\text{in}} = \begin{pmatrix} e^{-ik_{\uparrow}x} \\ 0 \end{pmatrix}, \tag{15}$$

$$\psi_r = \begin{pmatrix} r_{nf}\ e^{ik_{\uparrow}x} \\ r_{sf}\ e^{ik_{\downarrow}x} \end{pmatrix}, \tag{16}$$

where r_{sf} and r_{nf} are the coefficients for reflection with and without spin flip. These wave functions must be matched with those of Eq. (14).

Here we report the full solution for an arbitrary angle of rotation ϕ, not restricted to a multiple of π. For such situations the axis of magnetization on the left side of the domain wall may not not be parallel or antiparallel to the magnetization in the right side of the domain wall, where the carriers are injected. This solution is required in order to use these results to calculate the effect from piecewise constant domain walls. A transfer matrix approach is used to connect the wave functions at the edge of each piecewise constant region, until the entire domain wall has been traversed. In order to keep track of the change in spins all the way through the system, we apply the same transformation to the left lead as we do to the inside of the domain wall. Thus, the local "up" and "down" transmitted states along the magnetization of the left lead,

$$\varphi_t = \begin{pmatrix} Pe^{-ik_{\uparrow}x} \\ Qe^{-ik_{\downarrow}x} \end{pmatrix}, \tag{17}$$

become combinations of these states in the basis of the right lead:

$$\psi_t = R\varphi_t = \begin{pmatrix} \cos\left(\frac{\phi}{2}\right)Pe^{-ik_{\uparrow}x} + \sin\left(\frac{\phi}{2}\right)Qe^{-ik_{\downarrow}x} \\ -\sin\left(\frac{\phi}{2}\right)Pe^{-ik_{\uparrow}x} + \cos\left(\frac{\phi}{2}\right)Qe^{-ik_{\downarrow}x} \end{pmatrix}. \tag{18}$$

This form of ψ_t shows the orientation of the spins with respect to the magnetization on the incident side.

Setting up matching conditions for the wave functions and their derivatives at $x = 0$ and $x = -d$ yields eight boundary conditions:

$$1 + r_{nf} = N_1 i\phi k_1 d(B - A) + N_2 i\phi k_2 d(D - C), \tag{19}$$

$$-ik_{\uparrow} + ik_{\uparrow} r_{nf} = -N_1 i\phi k_1 d[ik_1(B + A)] - N_2 i\phi k_2 d[ik_2(D + C)] - \frac{\phi}{2d}[N_1\epsilon_1(A + B) + N_2\epsilon_2(C + D)], \tag{20}$$

$$r_{sf} = N_1\epsilon_1(A + B) + N_2\epsilon_2(C + D), \tag{21}$$

$$ik_{\downarrow} r_{sf} = N_1\epsilon_1 ik_1(A - B) + N_2\epsilon_2 ik_2(C - D) + \frac{\phi}{2d}[N_1 ik_1 d(B - A) + N_2 ik_2 d(D - C)], \tag{22}$$

$$\cos\left(\frac{\phi}{2}\right)Pe^{ik_{\uparrow}d} + \sin\left(\frac{\phi}{2}\right)Qe^{ik_{\downarrow}d} = \cos\left(\frac{\phi}{2}\right)[N_1 i\phi k_1 d(Be^{ik_1 d} - Ae^{-ik_1 d}) + N_2 i\phi k_2 d(De^{ik_2 d} - Ce^{ik_2 d})] + \sin\left(\frac{\phi}{2}\right)[N_1\epsilon_1(Ae^{-ik_1 d} + Be^{ik_1 d}) + N_2\epsilon_2(Ce^{-ik2d} + De^{ik_2 d})], \tag{23}$$

$$\begin{aligned} -ik_{\uparrow}\cos\left(\frac{\phi}{2}\right)Pe^{ik_{\uparrow}d} - ik_{\downarrow}\sin\left(\frac{\phi}{2}\right)Qe^{ik_{\downarrow}d} = {} & \cos\left(\frac{\phi}{2}\right)\Bigg[N_1\phi k_1^2 d(Be^{ik_1 d} + Ae^{-ik_1 d}) + N_2 ik_2 d(-ik_2)(De^{ik_2 d} + Ce^{-ik_2 d}) \\ & - \left(\frac{\phi}{2d}\right)N_1\epsilon_1(Ae^{-ik_1 d} + Be^{ik_1 d}) - \left(\frac{\phi}{2d}\right)N_2\epsilon_2(Ce^{-ik_2 d} + De^{ik_2 d})\Bigg] \\ & + \sin\left(\frac{\phi}{2}\right)\Bigg[N_1\epsilon_1 ik_1(Ae^{-ik_1 d} - Be^{ik_1 d}) + N_2\epsilon_2 ik_2(Ce^{-ik_2 d} - De^{ik_2 d}) \\ & + \left(\frac{\phi}{2d}\right)N_1 i\phi k_1 d(Be^{ik_1 d} - Ae^{-ik_1 d}) + \left(\frac{\phi}{2d}\right)N_2 i\phi k_2 d(De^{ik_2 d} - Ce^{-ik_2 d})\Bigg], \end{aligned} \tag{24}$$

$$-\sin\left(\frac{\phi}{2}\right)Pe^{ik_{\uparrow}d} + \cos\left(\frac{\phi}{2}\right)Qe^{ik_{\downarrow}d} = -\sin\left(\frac{\phi}{2}\right)\left[N_1 i\phi k_1 d\left(Be_{ik_1 d} - Ae^{-ik_1 d}\right) + N_2 i\phi k_2 d(De^{ik_2 d} - Ce^{-ik_2 d})\right] + \cos\left(\frac{\phi}{2}\right)[N_1\epsilon_1(Ae^{-ik_1 d} + Be^{ik_1 d}) + N_2\epsilon_2(Ce^{-ik_2 d} + De^{ik_2 d})], \tag{25}$$

$$ik_\uparrow \sin\left(\frac{\phi}{2}\right) P e^{ik_\uparrow d} - ik_\downarrow \cos\left(\frac{\phi}{2}\right) Q e^{ik_\downarrow d} = -\sin\left(\frac{\phi}{2}\right)\Big[N_1\phi k_1^2 d(Be^{ik_1 d} + Ae^{-ik_1 d}) + N_2 i\phi k_2 d(-ik_2)(De^{ik_2 d} + Ce^{-ik_2 d}) - \left(\frac{\phi}{2d}\right) N_1\epsilon_1(Ae^{-ik_1 d} + Be^{ik_1 d}) + \left(\frac{\phi}{2d}\right) N_2\epsilon_2(Ce^{-ik_2 d} + De^{ik_2 d})\Big] + \cos\left(\frac{\phi}{2}\right)\Big[N_1\epsilon_1 ik_1(Ae^{-ik_1 d} - Be^{ik_1 d}) + N_2\epsilon_2 ik_2(Ce^{-ik_2 d} - De^{ik_2 d}) + \left(\frac{\phi}{2d}\right) N_1 i\phi k_1 d(Be^{ik_1 d} - Ae^{-ik_1 d}) +)\left(\frac{\phi}{2d}\right))N_2 ik_2 d(De^{ik_2 d} - Ce^{-ik_2 d})\Big]. \tag{26}$$

These eight equations can be solved for r_{nf}, r_{sf}, Q, and P, which completely describe the incident, reflected, and transmitted wave functions shown in Eqs. (15), (16), and (18).

These coefficients also define the transmission and reflection probabilities for the system:

$$T_{nf} = \cos^2\left(\frac{\phi}{2}\right)|P|^2 + \sin^2\left(\frac{\phi}{2}\right)\frac{k_\downarrow}{k_\uparrow}|Q|^2, \tag{27}$$

$$T_{sf} = \sin^2\left(\frac{\phi}{2}\right)|P|^2 + \cos^2\left(\frac{\phi}{2}\right)\frac{k_\downarrow}{k_\uparrow}|Q|^2, \tag{28}$$

$$R_{nf} = |r_{nf}|^2, \tag{29}$$

$$R_{sf} = \frac{k_\downarrow}{k_\uparrow}|r_{sf}|^2. \tag{30}$$

C. Spin and charge current and spin torque from the analytic model

After obtaining the full wave functions for the entire system, we obtain[42] the charge current density $\mathbf{J}$ and spin current density $\mathbf{Q}$,

$$\mathbf{J} = \frac{e\hbar}{2im^*}[\psi^\dagger(\partial_x\psi) - (\partial_x\psi^\dagger)\psi]\hat{\mathbf{x}}, \tag{31}$$

$$\mathbf{Q} = \frac{\hbar}{2im^*}[\psi^\dagger\mathbf{S}(\partial_x\psi) - (\partial_x\psi^\dagger)\mathbf{S}\psi]. \tag{32}$$

The tensor $\mathbf{Q}$ has a flow direction in real space as well as a direction in spin space. The real-space flow direction lies along the direction of current ($\hat{x}$), and we write $\mathbf{Q}$ as a vector with components corresponding to the appropriate spin-space directions. As this spin current is not a conserved quantity, we can then define the spin torque per unit area as the amount of spin current lost to the domain wall during transport:[42]

$$\mathbf{N} = \mathbf{Q}_{\text{in}} + \mathbf{Q}_r - \mathbf{Q}_t. \tag{33}$$

Charge currents and spin torque can be calculated by integrating the transmission and reflection coefficients from Eq. (5) over the carrier population.

To analyze the situation in Fig. 1, we assume the left and right hand ferromagnetic regions to be reservoirs of spin-polarized carriers,[30] with chemical potentials $\mu_R = eV$ and $\mu_L = 0$. These reservoirs contain up spins on the right side, and local majority spins on the left side (these are down spins for a π wall and up spins for a 2π wall). We ignore the small density of minority carriers in the right hand lead, where the carriers are incident.

Time reversal symmetry stipulates that the amount of spin torque would be the same magnitude $\mathbf{N}$, but opposite direction, if carriers were injected from the left side instead of the right side, with no other changes to the system, and assuming perfect spin injection from each side. Thus the spin torque caused by injection of carriers from the right ($\mathbf{N}_R$) is a function of the majority population on the right side of the domain wall, and similarly for the left

$$\mathbf{N}_R = \mathbf{N} f_{R_{\text{maj}}}, \tag{34}$$

$$\mathbf{N}_L = \mathbf{N} f_{L_{\text{maj}}}. \tag{35}$$

The total spin torque is then the sum of the the torque from the left side, and the torque from the right side, integrated over the carrier population:

$$\mathbf{N}_{\text{tot}} = \int d^3k(\mathbf{N}_R + \mathbf{N}_L) = \int d^3k\big[\mathbf{N}\big(f_{R_{\text{maj}}} - f_{L_{\text{maj}}}\big)\big], \tag{36}$$

where the applicable distribution functions are

$$f_{R_{\text{maj}},L_{\text{mag}}} = \frac{1}{1 + e^{(\bar{E}_{\text{tot}} - \mu_{R,L})/\overline{k_B T}}},$$

and $\bar{E}_{\text{tot}} = \bar{E}_x + \bar{E}_t$ is the sum of the carrier kinetic energy associated with transport across the domain wall ($\bar{E}_x$), and the carrier kinetic energy in the transverse directions ($\bar{E}_t$). As the only difference between $f_{R_{\text{maj}}}$ and $f_{L_{\text{maj}}}$ is the chemical potential on each side, in equilibrium when $eV = 0$ then $N_{\text{tot}} = 0$. We define k_x and k_t from $\bar{E}_x$ and $\bar{E}_t$ as

$$k_x = \frac{1}{d}\sqrt{\bar{E}_x}, \quad k_t = \frac{1}{d}\sqrt{\bar{E}_t}. \tag{37}$$

The total torque can be evaluated from

$$\mathbf{N}_{\text{tot}} = \int_0^\infty dk_x \int_0^\infty dk_t k_t \int_0^{2\pi} d\theta \mathbf{N}(\bar{E}_x)\big[f_{R_{\text{maj}}}(\bar{E}_{\text{tot}}) - f_{L_{\text{maj}}}(\bar{E}_{\text{tot}})\big]. \tag{38}$$

Equation (38) includes the transverse orbital degrees of freedom for a three-dimensional Stoner model. Performing the integration over the two transverse directions,

$$\mathbf{N}_{\text{tot}} = \int_0^\infty \frac{d\bar{E}_x}{\sqrt{\bar{E}_x}}\mathbf{N}(\bar{E}_x)\ln\frac{1 + e^{(\overline{eV} - \bar{E}_x)/\overline{k_B T}}}{1 + e^{-\bar{E}_x/\overline{k_B T}}}. \tag{39}$$

Equation (39), with suitable choices for parameters, is used to calculate total spin torques. As with all the population-averaged quantities considered here (total spin current, total charge current, and spin torque), this integral is evaluated by

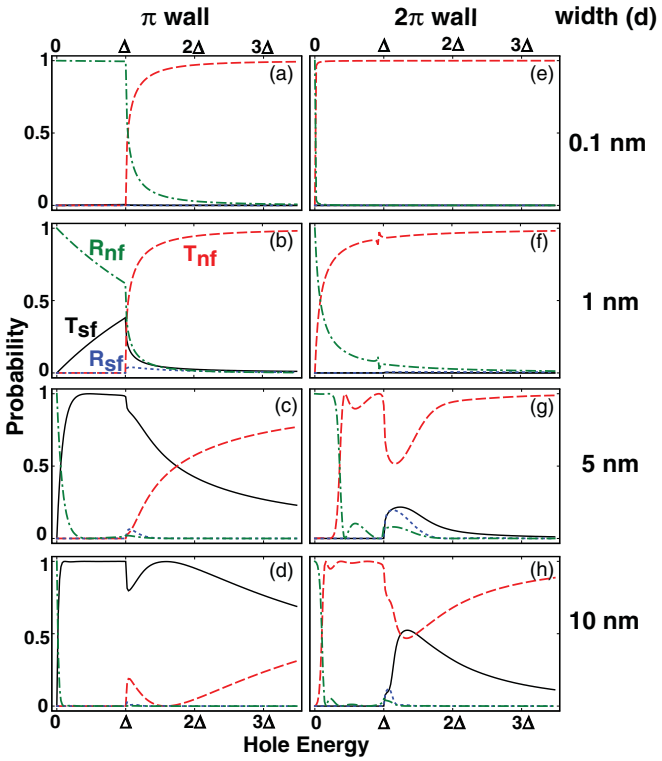

FIG. 3. (Color online) Probabilities for transmission through an abrupt domain wall with spin flip (T_{sf}, black solid line), transmission without spin flip (T_{nf}, red long-dashed line), reflection with spin flip (R_{sf}, blue short-dashed line) and reflection without spin flip (R_{nf}, green dot-dashed line) for (a)–(d) π and (e)–(h) 2π Néel walls with widths of 0.1, 1, 5, and 10 nm.

transforming the integration range extending to infinity to a finite range, using a change of variables, and then integrating using an adaptive step size.

III. RESULTS: TRANSMISSION AND REFLECTION COEFFICIENTS FOR DOMAIN WALLS

Calculations presented here will treat a model with spin splitting $\Delta = 100$ meV and valence hole effective mass $m^* = 0.45\, m_e$, where m_e is the mass of the bare electron. We assume a temperature of 110 K and a carrier density of $\sim 10^{19}$ cm^{-3}. For these parameters the magnetic semiconductor is nearly 100% spin polarized, and the effects found here are most visible. Although the results change quantitatively for different parameters (corresponding, e.g., to lower spin polarization), the qualitative trends we have identified are robust so long as the Fermi energy and the temperature are much less than the spin splitting.

Figure 3 shows calculated probabilities for transmission and reflection with and without spin flip for several thicknesses of abrupt π and 2π Néel walls (domain wall thickness presumably engineered by modifying film thickness and geometric shape), and Fig. 4 shows the charge current when an average over the carrier population is taken of the coefficients in Fig. 3. The thin wall and thick wall limits for 2π domain walls differ substantially from those of π domain walls. For thin walls the carriers effectively move through the domain

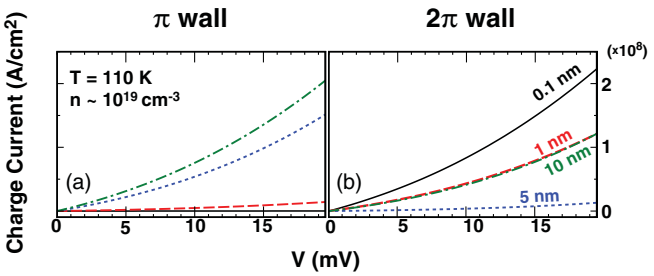

FIG. 4. (Color online) Charge current as a function of bias voltage for (a) π and (b) 2π walls. Curves correspond to different domain wall widths. Black solid line, 0.1 nm, red long-dashed line, 1 nm, blue short-dashed line, 5 nm, green dot-dashed line, 10 nm.

wall without changing their spin orientation, which leads to carrier reflection for the π domain wall as at low energy there are no final states on the other side with the correct spin orientation (and thus high resistance[30]). A thin 2π domain wall, however, will let the carriers through efficiently and thus have low resistance. As the thickness of a π domain wall increases, the spin-flip transmission monotonically increases [as shown for successively wider domain walls in Figs. 3(a)–3(d)], and the resistance drops, as shown in Fig. 4(a). As the thickness of a 2π domain wall increases initially from zero thickness, spin precession in the domain wall becomes more pronounced and carrier reflection is possible, so the resistance increases. However, in the limit of a very thick 2π domain wall the carriers will adiabatically follow the local magnetization and thus will be oriented once again parallel to the final magnetization, producing low resistance. Thus a finite thickness with maximal domain wall resistance should be expected for a 2π domain wall, as shown in Fig. 4(b).

IV. RESULTS: SPIN TORQUE IN π AND 2π DOMAIN WALLS

Figure 5 shows the calculated energy-resolved components of the spin torque from Eq. (33) for an abrupt domain wall. We focus on the energy region below the spin splitting Δ. In this region, the π wall graphs [Figs. 5(a)–5(d)] show large $\hat{x}$ and $\hat{y}$ torque components, with the largest values for both components appearing in the 1 nm wall [Fig. 5(b)]. In this energy region, the 2π wall graphs [Figs. 5(e)–5(h)] show very little torque for the 0.1 and 1 nm walls, but significant $\hat{x}$ and $\hat{y}$ torque components for the 5 and 10 nm walls, with the largest overall torque appearing in the 5 nm wall. We identify the spin torque as *adiabatic* [proportional to $\nabla \mathbf{M}(\mathbf{r})$, and thus parallel to $\hat{x}$] or *nonadiabatic* [proportional to $\mathbf{M}(\mathbf{r}) \times \nabla \mathbf{M}(\mathbf{r})$, parallel to $\hat{y}$], and find both components contribute significantly to the spin torque for both π and 2π walls.

Figure 6 shows the components of the total spin torque for each type of domain wall. We split the spin torque into the adiabatic $\hat{x}$ component and the nonadiabatic $\hat{y}$ component. For the π wall, we see that the sign of the torque components depends on the width of the domain wall. The adiabatic $\hat{x}$ component is positive for the smaller two domain wall widths, and negative for the larger two widths. The nonadiabatic $\hat{y}$ component is positive for the smallest and largest domain wall

widths, and negative for the middle two widths. We note that the adiabatic torque for the 5 and 10 nm walls for a π wall are nearly equal. This is consistent with the adiabatic torque saturating for large domain walls. For ballistic transport, a wide enough wall will result in nearly all the carriers precessing perfectly with the local magnetization inside the domain wall.

For the 2π wall, the adiabatic $\hat{x}$ component is always positive, and increases with the domain wall width. The nonadiabatic $\hat{y}$ component shows little spin torque for the 0.1 and 1 nm walls, and larger spin torque for the 5 and 10 nm walls, with the 5 nm wall being larger. The intermediate spin torque maximum is consistent with the concepts discussed above for Fig. 3, namely that the domain wall system reverts to almost total transmission of carriers without spin flipping for both very small walls (where the carriers can pass through without any change in spin orientation) and very wide walls (where the carriers precess along with the local magnetization and exit the domain wall with the magnetization orientation of the left lead, which has the same orientation as the right lead in a 2π wall).

Figure 7 examines this width dependence more closely, showing calculations for the individual torque components as well as the overall magnitude of the spin torque as a function of the abrupt domain wall width for a fixed applied voltage across the walls of 5 mV. The adiabatic $\hat{x}$ component of the spin torque in the abrupt π wall rises quickly to a maximum at a width near 2 nm, then falls off, changes sign, and stabilizes for large domain wall widths, confirming the saturation discussed above for Fig. 6. Similarly, the nonadiabatic $\hat{y}$ component reaches a

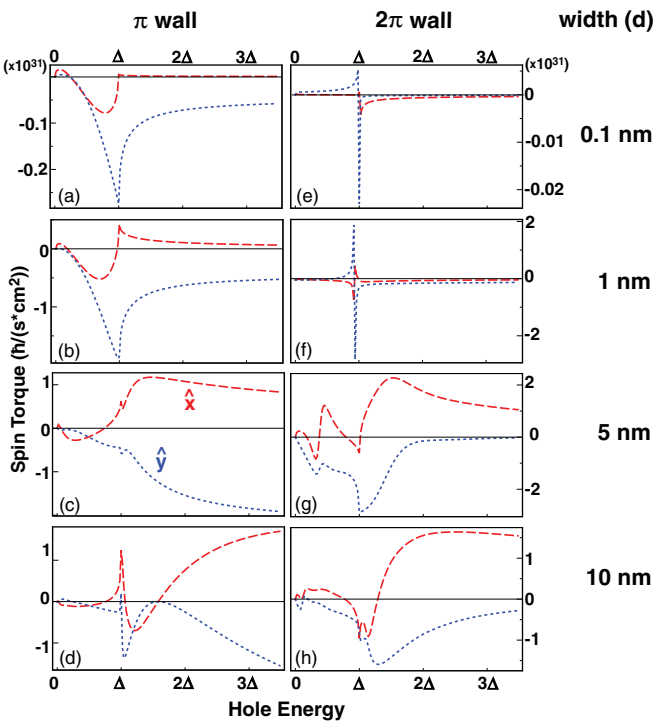

FIG. 5. (Color online) Spin torque components as a function of hole energy for π (a)–(d) and 2π (e)–(h) abrupt domain walls. Red long-dashed line is torque along $\hat{\mathbf{x}}$, blue short-dashed line is torque along $\hat{\mathbf{y}}$.

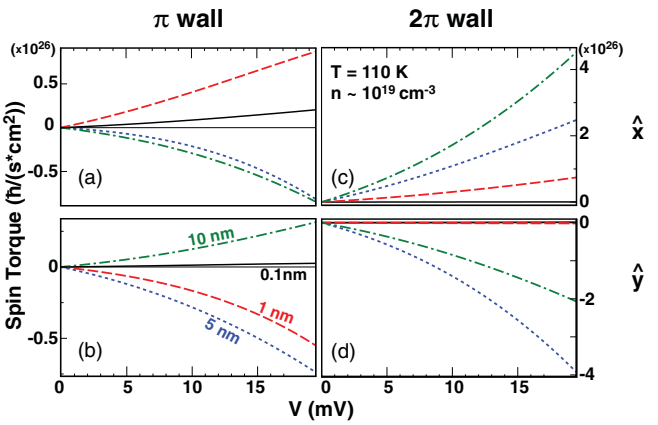

FIG. 6. (Color online) Spin torque components as a function of bias voltage for π (a) and (b) and 2π (c) and (d) abrupt domain walls. Color and line style is same as Fig. 4.

negative maximum near the same width, changes sign, and stabilizes for large domain wall widths. The magnitude of the spin torque shows that peak, along with the saturation at larger domain wall widths. The sharp jump from zero to that early peak is likely the result of the high reflection from narrow π walls. The carriers attempt to treat the thin wall as a narrow barrier and pass through without flipping their spins. However, there are no corresponding spin states on the other side of the π wall, resulting in a large amount of reflection. As this reflection vanishes for larger walls, the spin flip effect takes over, eventually producing a saturation.

For a 2π wall, the $\hat{x}$ component reaches a relative maximum near 9 nm and then appears to fall off slowly for larger widths. The $\hat{y}$ component has a peak that is around twice the magnitude of the $\hat{x}$ component at a width near 6 nm. The plot of the overall magnitude of the spin torque shows a small torque for the smallest width, larger torque in the intermediate widths, and a slow fall-off of the torque at larger widths. This is the same effect discussed above for Fig. 6 and holds true for both the adiabatic torque and the nonadiabatic torque. The torque rises slowly from zero as the domain walls become large enough for significant spin reorientation to occur, peaks

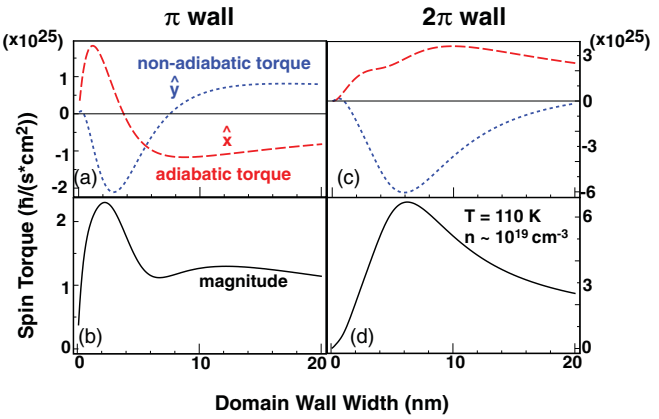

FIG. 7. (Color online) Spin torque components and magnitudes as a function of domain wall width for a π and 2π abrupt domain wall at $V = 5$ mV. Color and line style is same as Fig. 5.

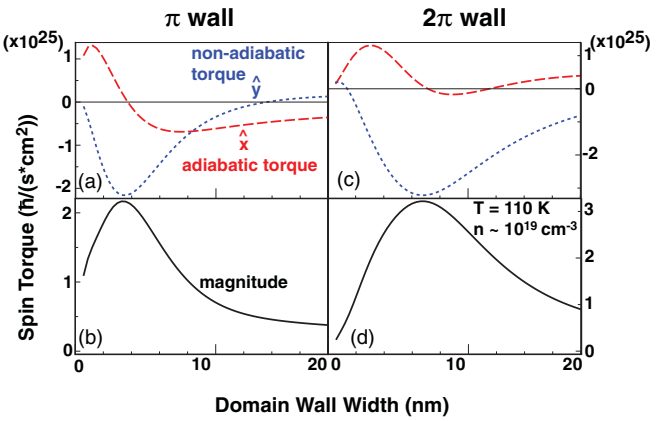

FIG. 8. (Color online) As Fig. 7 but for smooth domain walls.

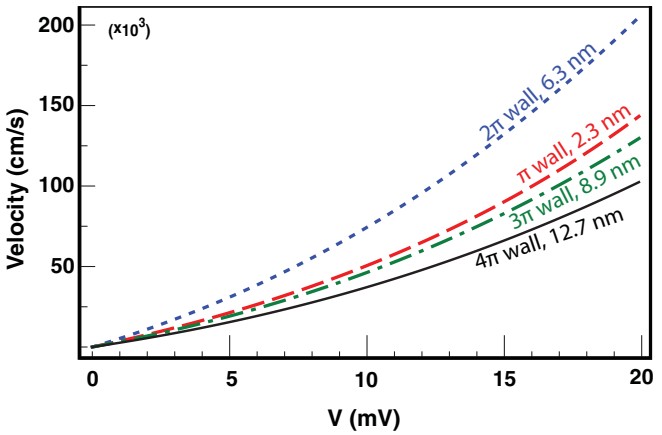

FIG. 9. (Color online) Calculated velocity at the abrupt domain wall width where spin torque is maximum for each of the π, 2π, 3π, and 4π walls.

at some intermediate width, and returns to zero in the limit where all the spins are precessing with the local magnetization.

We note that the peak spin torque magnitude for a 2π wall is nearly three times as large as the peak spin torque magnitude for a π wall. Additionally, this peak occurs for a 2π wall that is approximately three times as wide as a π wall at its corresponding peak. Why should the spin torque for a 2π wall exceed that of two π walls in succession? The spin torque is calculated assuming that the transverse spin orientation of carriers that have moved through the domain wall relaxes in the leads. For two π walls this transverse spin orientation is assumed to relax in between the two walls, and thus for two widely separated π walls the total spin torque should be just double that for a single π wall. For a 2π wall, however, there is no such relaxation after a π rotation of the magnetization, and thus the transverse spin orientation of the carriers can continue to be manipulated in the second half of the 2π wall. The crossover between two isolated π walls and a single 2π wall should be complex, for if the transverse spin orientation does not fully decay between the walls, then the total spin torque should depend on the precession of the transverse spin orientation of the carriers in the exchange field of the region in between the two π walls. Thus there should be intermediate separations between two π walls that result in *less* total spin torque than two isolated π walls. This study will be the subject of future study.

For a π abrupt domain wall the abrupt transition from constant to spatially varying exchange field generates a spin torque that is too large and that falls off too slowly (Fig. 7), compared with a smooth domain wall[24] (Fig. 8). In contrast, for the 2π wall, the spin torque does not change its qualitative dependence, although it is reduced for the smooth domain wall by about a factor of 2 across the entire range of wall widths. Although the nonadiabatic torque is disproportionately overestimated by an abrupt calculation for the π wall, it is the adiabatic torque that is disproportionately overestimated for the 2π domain wall. Thus the determination that the dominant torque for a 2π domain wall is the nonadiabatic torque, predicted from calculations for an abrupt domain wall, is even more valid for the smooth 2π domain wall. The common assumption of principally adiabatic torque for domain walls[22,24,43] (except for very narrow walls) breaks down for coherent transport through 2π domain walls, such as it does for unusual shape anisotropy or strong spin-orbit interaction.[44,45]

V. DOMAIN WALL VELOCITIES

For a wall undergoing an $n\pi$ rotation in magnetization from one side to the other, the domain wall velocity can be estimated as

$$v = \frac{g\mu_b}{nM_s}N, \tag{40}$$

where N is the total spin torque in $\hbar$ flips/(s cm^2) and M_s is the saturation magnetization of the material. Figure 9 shows the domain wall velocities for abrupt domain walls that result from the spin torque at the widths corresponding to peak spin torque for the π and 2π walls, as seen in Fig. 7, and also shows the peak domain wall velocity calculated for 3π and 4π walls. For each domain wall we first calculate the peak spin torque and the domain wall width producing that peak. This peak torque is then used in Eq. (40) to calculate a peak velocity.

We see in Fig. 9 that the 2π wall has a consistently larger velocity than the π wall does. Performing the same calculations for a 3π wall and a 4π wall, however, does not produce larger velocities than the one for the 2π wall. The

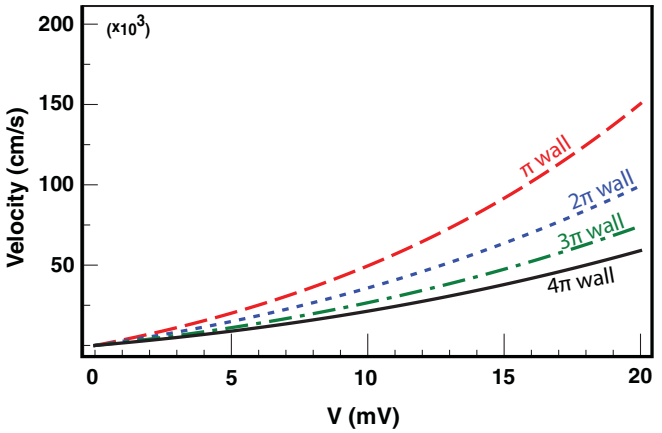

FIG. 10. (Color online) Same as Fig. 9 but for a smooth domain wall.

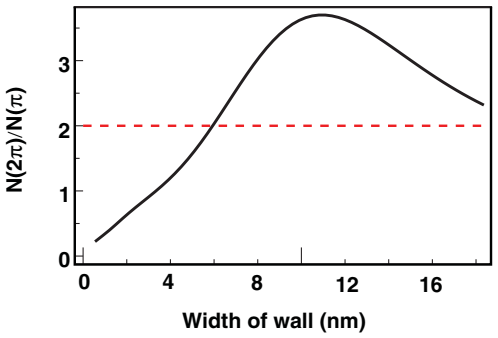

FIG. 11. (Color online) Ratio of the torque generated from current passing through a 2π domain wall to that generated from the same current passing through a π domain wall for a voltage of 5 mV. The dashed line indicates the ratio above which the 2π wall moves faster.

larger 2π wall velocity is easily attributed to the larger peak torque, as discussed above for Fig. 7. The smaller velocities for 3π and 4π walls point to an upper limit on the amount of torque in a domain wall. For a given domain wall configuration, at each point along the domain wall, there is a direction that produces the maximum amount of torque. When all the carriers are aligned in this fashion, the domain wall experiences its maximum torque. Walls with larger rotation angles have more angular momentum to turn over to move the domain wall. This means that a larger rotation angle should tend to correspond with a smaller domain wall velocity.

Figure 10 shows the velocity for a smooth domain wall. The reduction in overall torque for the 2π wall by a factor of 2 makes the domain wall velocity at peak velocity smaller than that of the π domain wall. However, for other regimes of domain wall thickness the 2π wall may move faster than the π wall. Shown below in Fig. 11 is the ratio of the spin torque of a 2π wall to that of a π wall; as it takes twice as much torque to move a 2π wall as fast as a π wall, Fig. 11 shows that for walls thicker than ~6–20 nm the 2π wall moves faster.

VI. CONCLUDING REMARKS

This treatment of coherent transport across domain walls has shown that the behavior of spin transport through domain walls is intrinsically nonlinear in voltage and magnetization rotation angle, for spin transport and torque both depend nonlinearly on the applied voltage, and the properties of a wall with twice the magnetization rotation (2π wall) are not related in any clear fashion to the properties of the π wall. The domain wall resistance to charge current follows different qualitative trends for the 2π domain wall than the π domain wall, leading to a maximum resistance at an intermediate wall thickness, as opposed to maximum resistance at zero thickness. An optimal-thickness 2π Néel wall experiences almost twice as much spin torque as an optimal thickness π domain wall for the same applied voltage, producing a comparable velocity for the 2π wall. At other thicknesses the velocity of the 2π wall exceeds that of a π wall. For the 2π wall there is an optimal width for achieving a maximum amount of spin torque, which should assist in understanding the time-dependent properties of domain walls in the presence of current, including potentially finding the fastest racers around a magnetic racetrack memory.[9]

ACKNOWLEDGMENT

This work was supported by an ARO MURI.

[1] J. C. Slonczewski, J. Magn. Magn. Mater. **159**, L1 (1996).
[2] L. Berger, Phys. Rev. B **54**, 9353 (1996).
[3] M. Tsoi, A. G. M. Jansen, J. Bass, W.-C. Chiang, M. Seck, V. Tsoi, and P. Wyder, Phys. Rev. Lett. **80**, 4281 (1998).
[4] E. B. Myers, D. C. Ralph, J. A. Katine, R. N. Louie, and R. A. Buhrman, Science **285**, 867 (1999).
[5] B. Özyilmaz, A. D. Kent, J. Z. Sun, M. J. Rooks, and R. H. Koch, Phys. Rev. Lett. **93**, 176604 (2004).
[6] M. Yamanouchi, D. Chiba, F. Matsukura, and H. Ohno, Nature (London) **428**, 539 (2004).
[7] X. Waintal and M. Viret, Europhys. Lett. **65**, 427 (2004).
[8] J. Grollier, P. Boulenc, V. Cros, A. Hamzić, A. Vaurès, and A. Fert, J. Appl. Phys. **95**, 6777 (2004).
[9] S. S. P. Parkin, M. Hayashi, and L. Thomas, Science **320**, 190 (2008).
[10] I. M. Miron, P.-J. Zermatten, G. Gaudin, S. Auffret, B. Rodmacq, and A. Schuhl, Phys. Rev. Lett. **102**, 137202 (2009).
[11] S. Lepadatu, A. Vanhaverbeke, D. Atkinson, R. Allenspach, and C. H. Marrows, Phys. Rev. Lett. **102**, 127203 (2009).
[12] T. Tserkovnyak, A. Brataas, and G. E. W. Bauer, J. Magn. Magn. Mater. **320**, 1282 (2008).
[13] S. Kasai, Y. Nakatani, K. Kobayashi, H. Kohno, and T. Ono, Phys. Rev. Lett. **97**, 107204 (2006).
[14] J. C. Sankey, P. M. Braganca, A. G. F. Garcia, I. N. Krivorotov, R. A. Buhrman, and D. C. Ralph, Phys. Rev. Lett. **96**, 227601 (2006).
[15] A. A. Tulapurkar, Y. Suzuki, A. Fukushima, H. Kubota, H. Maehara, K. Tsunekawa, D. D. Djayaprawira, N. Watanabe, and S. Yuasa, Nature (London) **438**, 339 (2005).
[16] G. D. Fuchs, J. C. Sankey, V. S. Pribiag, L. Qian, P. M. Braganca, A. G. F. Garcia, E. M. Ryan, Z.-P. Li, D. C. Ralph, and R. A. Buhrman, Appl. Phys. Lett. **91**, 062507 (2007).
[17] T. Balashov, A. F. Takács, M. Däne, A. Ernst, P. Bruno, and W. Wulfhekel, Phys. Rev. B **78**, 174404 (2008).
[18] M. Yamanouchi, D. Chiba, F. Matsukura, T. Dietl, and H. Ohno, Phys. Rev. Lett. **96**, 096601 (2006).
[19] A. Yamaguchi, T. Ono, S. Nasu, K. Miyake, K. Mibu, and T. Shinjo, Phys. Rev. Lett. **92**, 077205 (2004).
[20] A. N. Morozovska, S. V. Kalinin, E. A. Eliseev, V. Gopalan, and S. V. Svechnikov, Phys. Rev. B **78**, 125407 (2008).
[21] A. K. Nguyen, H. J. Skadsem, and A. Brataas, Phys. Rev. Lett. **98**, 146602 (2007).

[22] A. Thiaville, Y. Nakatani, J. Miltat, and Y. Suzuki, Europhys. Lett. **69**, 990 (2005).
[23] S. E. Barnes and S. Maekawa, Phys. Rev. Lett. **95**, 107204 (2005).
[24] J. Xiao, A. Zangwill, and M. D. Stiles, Phys. Rev. B **73**, 054428 (2006).
[25] V. K. Dugaev, V. R. Vieira, P. D. Sacramento, J. Barnás, M. A. N. Araújo, and J. Berakdar, Phys. Rev. B **74**, 054403 (2006).
[26] G. Tatara and H. Kohno, Phys. Rev. Lett. **92**, 086601 (2004).
[27] H. Ohno and T. Dietl, J. Magn. Magn. Mater. **320**, 1293 (2008).
[28] C. B. Muratov and V. V. Osipov, J. Appl. Phys. **104**, 053908 (2008).
[29] D. O. Smith and K. J. Harte, J. Appl. Phys. **33**, 1399 (1962).
[30] G. Vignale and M. E. Flatté, Phys. Rev. Lett. **89**, 098302 (2002).
[31] M. Deutsch, G. Vignale, and M. Flatté, J. Appl. Phys. **96**, 7424 (2004).
[32] D. A. Allwood, G. Xiong, C. C. Faulkner, D. Atkinson, D. Petit, and R. P. Cowburn, Science **309**, 1688 (2005).
[33] T. Ono and Y. Nakatani, Appl. Phys. Exp. **1**, 061301 (2008).
[34] P. M. Levy and S. Zhang, Phys. Rev. Lett. **79**, 5110 (1997).
[35] S. Chikazumi, *Physics of Ferromagnetism*, 2nd ed., International Series of Monographs on Physics, Vol. 94 (Oxford University Press, Oxford, 1997).
[36] A. K. Nguyen, R. V. Shchelushkin, and A. Brataas, Phys. Rev. Lett. **97**, 136603 (2006).
[37] R. Oszwałdowski, J. A. Majewski, and T. Dietl, Phys. Rev. B **74**, 153310 (2006).
[38] K. M. D. Hals, A. K. Nguyen, and A. Brataas, Phys. Rev. Lett. **102**, 256601 (2009).
[39] D. Awschalom, N. Samarth, and D. Loss (eds.), *Semiconductor Spintronics and Quantum Computation* (Springer, New York, 2002).
[40] H. Schomig, A. Forchel, S. Halm, G. Bacher, J. Puls, and F. Henneberger, Appl. Phys. Lett. **84**, 2826 (2004).
[41] M. Calvo, Phys. Rev. B **18**, 5073 (1978).
[42] D. C. Ralph and M. D. Stiles, J. Magn. Magn. Mater. **320**, 1190 (2008).
[43] S. Zhang and Z. Li, Phys. Rev. Lett. **93**, 127204 (2004).
[44] O. Boulle, J. Kimling, P. Warnicke, M. Kläui, U. Rüdiger, G. Malinowski, H. J. M. Swagten, B. Koopmans, C. Ulysse, and G. Faini, Phys. Rev. Lett. **101**, 216601 (2008).
[45] I. Garate, K. Gilmore, M. D. Stiles, and A. H. MacDonald, Phys. Rev. B **79**, 104416 (2009).